A robust inverse scattering method based on shape optimization

Thomas Bonnafont
Lab-STICC, UMR CNRS 6285
ENSTA Bretagne
Brest, France
thomas.bonnafont@ensta-bretagne.fr

Fabien Caubet
E2S UPPA, CNRS, LMAP, UMR 5142
Pau, France
fabien.caubet@univ-pau.fr

***Abstract*—In this work, we develop a robust method to retrieve the shape of a metallic object from partial electromagnetic measurements containing noise. The numerical resolution of the inverse problem is tackled through parametric shape optimization. To make the method robust, the expectation of the Kohn-Vogelius cost function is minimized here: the key point is to use the so-called Karhunen-Loève expansion in order to obtain an explicit deterministic shape gradient. Then, the optimization problem is solved using a Nesterov gradient scheme. Numerical tests are provided to highlight the advantages and the efficiency of the proposed method.**

***Index Terms*—inverse scattering, shape optimization, robust method, Karhunen-Loève decomposition, Nesterov scheme, Kohn-Vogelius functional**

I. Introduction

Retrieving the shape of an obstacle using electromagnetic measurements is a topic of major interest for many applications in defense, health monitoring, or geoscience. Many techniques have been developed to tackle this inverse problem (see, e.g., [1]–[4]).

For example, inverse synthetic-aperture radars use the Doppler effect introduced by the movement of the target to compute a high-resolution image of the latter [1], [3].

More recently shape optimization techniques have received more attention from the inverse scattering community (see, e.g., [5]–[7] in acoustics and [2], [4], [8] in electromagnetics). The idea is to modify the shape of an initial object iteratively to minimize an objective functional and obtain the field that induced the observed measurements. The accuracy of the reconstruction is measured by a suitable metric. Most of the results have been obtained considering a least squares functional, using for example topological [6] or level-set [4], [7] shape optimization methods. Usually, the shape of the object is modified using a conventional gradient descent scheme, after the computation of the shape gradient. Notice that the *robustness* (which means the sensitivity of the method with respect to some errors on the data) has only been tested numerically by adding noise to the measurements.

This paper aims to provide a robust inverse scattering method based on shape optimization. We highlight the recent work [9], where a robust method is developed to reconstruct an obstacle in an elastic medium: here we want to adapt this procedure in the inverse scattering context. Besides, we focus here on the so-called Kohn-Vogelius functional (see, e.g., [10], [11]) in the optimization process since it has been shown to be more robust. Furthermore, to accelerate the reconstruction a Nesterov gradient scheme (see [9]) is used instead of a conventional gradient descent.

The remainder of this paper is organized as follows. Section II focuses on the inverse model. First, some notations and the direct problem are introduced. Second, the inverse scattering problem with noisy measurements we are studying is introduced. In Section III, we derive a robust shape optimization technique to retrieve the shape of the target. To do so the inverse problem is rewritten as an optimization one, where the expectation of the Kohn-Vogelius functional is used as the cost function. Using the Karhunen-Loève expansion, a deterministic expression of the functional is then calculated. The latter is then minimized using a Nesterov gradient scheme. Section IV highlights the advantages of the proposed robust method through numerical tests under different scenarios. Section V concludes the paper and gives perspectives for improvements and future works.

II. The inverse model containing uncertainties

A. Notations and direct problem

Throughout this paper, the following notations are used. The vectors are denoted in bold, such as $\boldsymbol{V}$. In particular, the exterior unit normal vector of a domain is denoted by $\mathbf{n}$. We denote by $\partial_{\mathrm{n}} u$ the normal derivative for a smooth function u.

For $z \in \mathbb{C}$, its real and imaginary parts are denoted by $\Re(z)$ and $\Im(z)$, respectively. Its complex conjugate is denoted by $\bar{z}$. Besides, we denote by j the imaginary unit here. For u and v two complex-valued functions the usual scalar product is used:

$$< u, v >= \int u\bar{v}.$$

In this paper, we assume an $\exp(j\Phi t)$ time dependence, with $\Phi = 2\pi f$ the angular frequency and f the frequency. The wave number is denoted by k with $k = \frac{2\pi f}{c}$, and c is the speed of light in the considered media.

Let $\mathcal{D} \subset \mathbb{R}^2$ be a nonempty connected bounded Lipschitz domain. We assume that its boundary $\partial\mathcal{D}$ is divided into two

nonempty open subdomains (with a strictly positive measure) as follows: $\partial\mathcal{D} = \overline{\Gamma_{\rm m} \cup \Gamma_{\rm c}}$, $\Gamma_{\rm m}$ the part where we can make some measurements and $\Gamma_{\rm c}$ its complementary in $\partial\mathcal{D}$.

We consider the scattering of a given Perfectly Metallic Conductor (PEC), denoted by $\mathcal{O}$, with a smooth boundary $\partial\mathcal{O}$, strictly included in the domain $\mathcal{D}$. We assume that in $\mathcal{D}\backslash\overline{\mathcal{O}}$ (which is assumed to be open and simply connected), the permittivity and the permeability are respectively given by $\varepsilon = \varepsilon_0$ and $\mu = \mu_0$: it corresponds to the free-space.

The incident and scattered waves are denoted by $u_{\rm i}$ and $u_{\rm s}$, respectively. The incident wave is assumed to be a plane wave with an angle of incidence from the x-axis denoted by $\theta_{\rm i}$, and an amplitude of $u_{\rm i_0}$. The total field u corresponds to the sum of both such that

$$u = u_{\rm i} + u_{\rm s}.$$

The notations are pictured in Fig. 1, with the target $\mathcal{O}$ in red.

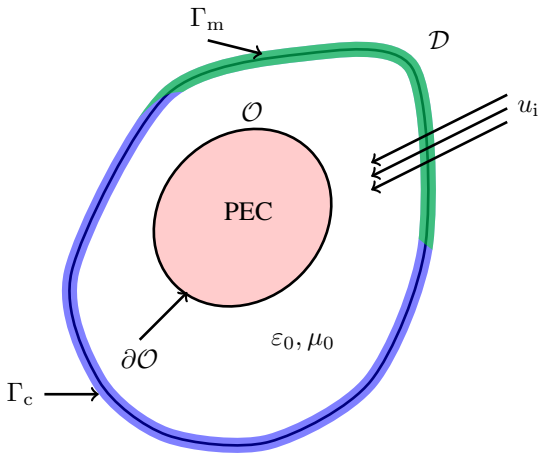

Fig. 1: Example of the considered domain $\mathcal{D}$ with the scatterer $\mathcal{O}$ (in red) inside.

Since the object is considered to be a PEC, the mathematical formulation of the forward problem is as follows:

$$\left\{\begin{array}{rcll} \Delta u + k^2 u &=& 0 & \text{in } \mathcal{D}\backslash\overline{\mathcal{O}}, \\ \partial_{\rm n} u + jku &=& h & \text{on } \partial\mathcal{D}, \\ u &=& 0 & \text{on } \partial\mathcal{O}. \end{array}\right. \tag{1}$$

In this problem, we define

$$h = j(k - \mathbf{k}_{\rm i}(\theta_{\rm i}) \cdot \mathbf{n}) u_{\rm i_0} \exp(-j\mathbf{k}_{\rm i}(\theta_{\rm i}) \cdot \mathbf{r}),$$

where $\mathbf{k}_{\rm i}$ corresponds to the incident wave vector given by

$$\mathbf{k}_{\rm i} = -k\,(\cos(\theta_{\rm i}), \sin(\theta_{\rm i})),$$

and $\mathbf{r} = (x_X, y_X)$ is the position of a point $X \in \mathcal{D}$. This problem corresponds to the bounded formulation of the open scattering problem, where the boundary condition on $\partial\mathcal{D}$ is an absorbing boundary condition introduced such that the field respects the Sommerfeld condition.

B. The studied inverse scattering problem

The aim of this work is to numerically solve the corresponding inverse obstacle problem, from boundary measurements. More precisely, we assume that a measurement $u = g$ is known on $\Gamma_{\rm m}$ and we want to reconstruct the PEC $\mathcal{O}$. Thus, the inverse problem can be formulated as:

Find $\mathcal{O}$ and the solution $u \in \mathrm{H}^1(\mathcal{D}\backslash\overline{\mathcal{O}})$ such that

$$\left\{\begin{array}{rcll} \Delta u + k^2 u &=& 0 & \text{in } \mathcal{D}\backslash\overline{\mathcal{O}}, \\ \partial_{\rm n} u + jku &=& h & \text{on } \partial\mathcal{D}, \\ u &=& g & \text{on } \Gamma_{\rm m}, \\ u &=& 0 & \text{on } \partial\mathcal{O}. \end{array}\right.$$

In view of concrete applications, the main aim and novelty of this work (which follows our previous work [11]) is to take into account the uncertainties contained in the measurement g and in the incident wave (and thus in h). More rigorously, let $(\Omega, \mathcal{S}, \mathbb{P})$ be a complete probability space. We assume that $g : \Gamma_{\rm m} \times \Omega \longrightarrow \mathbb{R}$ and $h : \partial\mathcal{D} \times \Omega \longrightarrow \mathbb{C}$ are two random fields belonging to the space $\mathrm{L}^2_{\mathbb{P}}(\Omega, \mathrm{H}^{1/2}(\Gamma_{\rm m}))$ and $\mathrm{L}^2_{\mathbb{P}}(\Omega, \mathrm{H}^{-1/2}(\partial\mathcal{D}))$, respectively. Then, for a given $\omega \in \Omega$, the inverse problem can be rewritten as

Find $\mathcal{O}$ and the solution $u(\omega) \in \mathrm{H}^1(\mathcal{D}\backslash\overline{\mathcal{O}})$ such that

$$\left\{\begin{array}{rcll} \Delta u(\omega) + k^2 u(\omega) &=& 0 & \text{in } \mathcal{D}\backslash\overline{\mathcal{O}}, \\ \partial_{\rm n} u(\omega) + jku(\omega) &=& h(\omega) & \text{on } \partial\mathcal{D}, \\ u(\omega) &=& g(\omega) & \text{on } \Gamma_{\rm m}, \\ u(\omega) &=& 0 & \text{on } \partial\mathcal{O}. \end{array}\right. \tag{2}$$

Notice that $u(\omega)$ is thus a random field.

The objective is to ensure a robust reconstruction of the PEC, even if the measurements contain errors. To do so, the strategy is to, as usual, consider an optimization problem but instead of minimizing a well-chosen cost function we aim to minimize its expectation. The following section explains in more detail this procedure.

III. A robust shape optimization method

A. An optimization reformulation

In order to numerically solve the above inverse problem (2), we have in mind the classical and natural idea which consists in minimizing a cost functional. We here focus on the so-called Kohn-Vogelius functional (as studied in [11]) which is, in this context, a random process given, for $\omega \in \Omega$, by

$$\mathcal{K}(\mathcal{O}, \omega) = \frac{1}{2} \int_{\mathcal{D}\backslash\overline{\mathcal{O}}} |\nabla(u_{\rm D}(\omega) - u_{\rm R}(\omega))|^2,$$

where the random fields $u_{\rm D}(\omega)$ and $u_{\rm R}(\omega)$ respectively solve

$$\left\{\begin{array}{rcll} \Delta u_{\rm D}(\omega) + k^2 u_{\rm D}(\omega) &=& 0 & \text{in } \mathcal{D}\backslash\overline{\mathcal{O}}, \\ \partial_{\rm n} u_{\rm D}(\omega) + jku_{\rm D}(\omega) &=& h(\omega) & \text{on } \Gamma_{\rm c}, \\ u_{\rm D}(\omega) &=& g(\omega) & \text{on } \Gamma_{\rm m}, \\ u_{\rm D}(\omega) &=& 0 & \text{on } \partial\mathcal{O}, \end{array}\right.$$

and

$$\left\{\begin{array}{rcll} \Delta u_{\rm R}(\omega) + k^2 u_{\rm R}(\omega) &=& 0 & \text{in } \mathcal{D}\backslash\overline{\mathcal{O}}, \\ \partial_{\rm n} u_{\rm R}(\omega) + jku_{\rm R}(\omega) &=& h(\omega) & \text{on } \partial\mathcal{D}, \\ u_{\rm R}(\omega) &=& 0 & \text{on } \partial\mathcal{O}. \end{array}\right.$$

The aim is to come back to a deterministic problem, in order to avoid stochastic methods which can be very costly in a shape optimization process. To do this, we choose to minimize the expectation of the shape functional $\mathcal{K}$. Thus, we now want to minimize the following functional

$$\mathfrak{K}(\mathcal{O}) = \mathbb{E}(\mathcal{K}(\mathcal{O}, \omega)).$$

Notice that all the results presented in this work can be easily adapted to the classical least squares functional.

The key point is to assume that the measured Dirichlet data g and the Robin boundary condition h are perturbed by a finite-dimensional noise of the form

$$g(x,\omega) = g_0(x) + \sum_{i=1}^{M} g_i(x) Y_i(\omega)$$

and

$$h(x,\omega) = h_0(x) + \sum_{i=1}^{M} h_i(x) Y_i(\omega),$$

where $M > 0$ is a given integer, where $g_i \in \mathrm{H}^{1/2}(\Gamma_{\mathrm{m}})$ and $h_i \in \mathrm{H}^{-1/2}(\partial\mathcal{D})$, $i = 0, \cdots, M$, are deterministic, and where the random variables Y_i are independent and identically distributed random variables, $Y_i \sim Y$, are centered, $\mathbb{E}(Y) = 0$, and normalized, $\mathbb{V}(Y) = 1$.

Notice that this assumption concerning g is natural having in mind several independent measurements from which we can derive the sample mean and the sample covariance. Then, such an expression can be derived from by means of the Karhunen–Loève expansion (see, e.g., [9] for details). The same remark holds for the incident wave, and then for h.

Then, the linearity of the Helmholtz equations and the superposition principle lead

$$u_{\mathrm{D}}(x,\omega) = u_{\mathrm{D}_0}(x) + \sum_{i=1}^{M} u_{\mathrm{D}_i}(x) Y_i(\omega)$$

and

$$u_{\mathrm{R}}(x,\omega) = u_{\mathrm{R}_0}(x) + \sum_{i=1}^{M} u_{\mathrm{R}_i}(x) Y_i(\omega),$$

where, for all $i = 0, \ldots, M$, u_{D_i} and u_{R_i} solve respectively

$$\left\{ \begin{array}{rcll} \Delta u_{\mathrm{D}_i} + k^2 u_{\mathrm{D}_i} & = & 0 & \text{in } \mathcal{D}\backslash\overline{\mathcal{O}}, \\ \partial_{\mathrm{n}} u_{\mathrm{D}_i} + jk u_{\mathrm{D}_i} & = & h_i & \text{on } \Gamma_{\mathrm{c}}, \\ u_{\mathrm{D}_i} & = & g_i & \text{on } \Gamma_{\mathrm{m}}, \\ u_{\mathrm{D}_i} & = & 0 & \text{on } \partial\mathcal{O}, \end{array} \right. \tag{3}$$

and

$$\left\{ \begin{array}{rcll} \Delta u_{\mathrm{R}_i} + k^2 u_{\mathrm{R}_i} & = & 0 & \text{in } \mathcal{D}\backslash\overline{\mathcal{O}}, \\ \partial_{\mathrm{n}} u_{\mathrm{R}_i} + jk u_{\mathrm{R}_i} & = & h_i & \text{on } \Gamma_{\mathrm{c}}, \\ u_{\mathrm{R}_i} & = & 0 & \text{on } \partial\mathcal{O}. \end{array} \right. \tag{4}$$

B. Estimation of the expected value

The aim is first to find an expression of the expected value that is of the functional $\mathfrak{K}(\mathcal{O})$. Since $|\nabla(u_{\mathrm{D}} - u_{\mathrm{R}})|^2$ is a positive function, we can use Fubini's theorem to obtain

$$\begin{aligned} \mathfrak{K}(\mathcal{O}) &= \frac{1}{2}\int_{\Omega}\int_{\mathcal{D}\backslash\overline{\mathcal{O}}} |\nabla(u_{\mathrm{D}}(\omega) - u_{\mathrm{R}}(\omega))|^2 \mathrm{d}x\mathrm{d}\mathbb{P}(\omega) \\ &= \frac{1}{2}\int_{\mathcal{D}\backslash\overline{\mathcal{O}}}\int_{\Omega} |\nabla(u_{\mathrm{D}}(\omega) - u_{\mathrm{R}}(\omega))|^2 \mathrm{d}\mathbb{P}(\omega)\mathrm{d}x. \end{aligned}$$

Then some computations give

$$\begin{aligned} |\nabla(u_{\mathrm{D}}(\omega) - u_{\mathrm{R}}(\omega))|^2 &= |\nabla(u_{\mathrm{D}_0} - u_{\mathrm{R}_0})|^2 \\ &+ 2\sum_{i=1}^{M} \nabla(u_{\mathrm{D}_0} - u_{\mathrm{R}_0}) \cdot \overline{\nabla(u_{\mathrm{D}_i} - u_{\mathrm{R}_i})} Y_i(\omega) \\ &+ \sum_{i,j=1}^{M} \nabla(u_{\mathrm{D}_i} - u_{\mathrm{R}_i}) \cdot \overline{\nabla(u_{\mathrm{D}_{\mathrm{j}}} - u_{\mathrm{R}_{\mathrm{j}}})} Y_i(\omega) Y_j(\omega). \end{aligned}$$

Taking into account that Y_i are independent, identically distributed random variables centered and normalized, we obtain

$$\begin{aligned} \mathfrak{K}(\mathcal{O}) = \frac{1}{2}\int_{\mathcal{D}\backslash\overline{\mathcal{O}}} |\nabla(u_{\mathrm{D}_0} - u_{\mathrm{R}_0})|^2 \\ + \frac{1}{2}\sum_{i=1}^{M}\int_{\mathcal{D}\backslash\overline{\mathcal{O}}} |\nabla(u_{\mathrm{D}_i} - u_{\mathrm{R}_i})|^2. \end{aligned} \tag{5}$$

This expression is now deterministic and thus we can follow some classical shape optimization strategies to minimize it. It should be noted that when minimizing (5), the second part of the expression intends to eliminate all components of the noise (except its mean), thereby leading to more robust results.

C. Shape gradient and optimization algorithm

In order to minimize the above Kohn-Vogelius functional $\mathfrak{K}$, we aim to use a gradient type algorithm and thus we have to compute its *shape gradient*. Roughly speaking, the shape gradient of $\mathfrak{K}$ at $\mathcal{O}$ is obtained by computing $\lim_{\eta\to 0} \dfrac{\mathfrak{K}(\mathcal{O}_\eta) - \mathfrak{K}(\mathcal{O})}{\eta}$, where $\mathcal{O}_\eta = (\mathbf{I} + \eta\boldsymbol{V})(\mathcal{O})$ is a perturbation of the domain $\mathcal{O}$, with $\eta \neq 0$ and $\boldsymbol{V}$ a direction perturbation (see, e.g., [12], [13] for details on the notion of shape derivatives). Note that results on the existence of the shape derivatives concerning our problem have been proven in [2].

Using the expression (5), the computation of the shape gradient of $\mathfrak{K}$ becomes analogous to what we have done in [11]. After some tedious computations, for given admissible shape $\mathcal{O}$ and admissible perturbation $\boldsymbol{V}$, we obtain the following useful expression:

$$\begin{aligned} \nabla\mathfrak{K}(\mathcal{O}) \cdot \boldsymbol{V} = \Re\Bigg(\int_{\partial\mathcal{O}} (\boldsymbol{V}\cdot\mathbf{n}) \sum_{i=0}^{M} \Bigg(\frac{1}{2}|\nabla(u_{\mathrm{D}_i} - u_{\mathrm{R}_i})|^2 \\ + \partial_{\mathrm{n}} u_{\mathrm{D}_i} \Big(\partial_{\mathrm{n}} z_i - \partial_{\mathrm{n}}(\overline{u_{\mathrm{D}_i} - u_{\mathrm{R}_i}}) \Big) - \partial_{\mathrm{n}} w_i \partial_{\mathrm{n}} u_{\mathrm{R}_i} \Bigg) \Bigg), \end{aligned} \tag{6}$$

where, for all $i = 1, \dots, M$, u_{D_i} and u_{R_i} respectively solve the above systems (3) and (4), and w_i and z_i are the solutions to the respective following adjoint problems

$$\left\{\begin{array}{rcll} \Delta w_i + k^2 w_i & = & -k^2(\overline{u_{\mathrm{D}_i} - u_{\mathrm{R}_i}}) & \text{in } \mathcal{D}\backslash\overline{\mathcal{O}}, \\ \partial_{\mathrm{n}} w_i + jk w_i & = & -jk(\overline{u_{\mathrm{D}_i} - u_{\mathrm{R}_i}}) & \text{on } \partial\mathcal{D}, \\ w_i & = & 0 & \text{on } \partial\mathcal{O}, \end{array}\right. \tag{7}$$

and

$$\left\{\begin{array}{rcll} \Delta z_i + k^2 z_i & = & -k^2(\overline{u_{\mathrm{D}_i} - u_{\mathrm{R}_i}}) & \text{in } \mathcal{D}\backslash\overline{\mathcal{O}}, \\ \partial_{\mathrm{n}} z_i + jk z_i & = & \partial_{\mathrm{n}}(\overline{u_{\mathrm{D}_i} - u_{\mathrm{R}_i}}) & \text{on } \Gamma_{\mathrm{c}}, \\ z_i & = & 0 & \text{on } \Gamma_{\mathrm{m}}, \\ z_i & = & 0 & \text{on } \partial\mathcal{O}. \end{array}\right. \tag{8}$$

Notice that, in order to compute its shape gradient, we have to solve, at each iteration, $4M$ partial differential equations of the same type. Indeed, only the source term is different, thus it is not too expensive numerically.

D. Numerical inversion strategy

From now on, the aim is to approach the solution to the following optimization problem

$$\min_{\mathcal{O}\in\mathcal{U}_{\mathrm{ad}}} \mathfrak{K}(\mathcal{O}),$$

on a set $\mathcal{U}_{\mathrm{ad}}$ of admissible shapes.

We follow the same strategy as in [11], that is we consider a truncated Fourier series parametrization for the boundary of the object $\mathcal{O}$:

$$\begin{aligned}\partial\mathcal{O} = \Big\{ & (x_{\mathrm{c}}, y_{\mathrm{c}})^t + r(\cos(\Theta), \sin(\Theta))^t \\ & + \sum_{n\geq 1}^{N} (a_n, b_n)(\cos(n\Theta), \sin(n\Theta))^t (\cos(\Theta), \sin(\Theta))^t, \\ & \qquad \Theta \in [0, 2\pi[\Big\},\end{aligned}$$

where the upper script ^{t} denotes the transpose, $(x_{\mathrm{c}}, y_{\mathrm{c}})$ is the center, r is the radius, and where $N \in \mathbb{N}^*$. Moreover, we have performed a Nesterov gradient descent scheme with restart (see [9] for details on the algorithm, see also [7]), using the shape gradient given by (6). Finally, to overcome the instability of the inverse problem, the Fourier coefficients are added one after another, after a given number of iterations.

IV. Numerical tests

To conclude this work, we perform some numerical tests in order to highlight the efficiency of the proposed method, using the PDE solver Freefem++ (see [14]). For those tests, artificial data are computed from the direct problem (1) using a P2 finite element method on a coarse mesh. In order to avoid the so-called *inverse crime*, Problems (3), (4), (7) and (8), needed in the optimization process (to compute the descent direction using the above shape gradient expression), are solved using P1 finite elements on a less coarse mesh.

A. Framework of the simulations

In all the simulations, $\mathcal{D}$ is the square $]-1,1[\times]-1,1[$ and the initial guess $\mathcal{O}_0$ is a disk of center $(-0.1, 0.1)$ and radius 0.4 pictured in yellow line below. We assume that the measurements are performed on the top, bottom, and right boundaries of $\mathcal{D}$, pictured in green below (which represent Γ_{m}). We aim to retrieve the *real PEC* given by

$$\begin{aligned}\partial\mathcal{O} = \Big\{ & \big(x = 0.15 + 0.65\cos(\Theta) - 0.25\cos^2(\Theta) \\ & - 0.15\sin(\Theta)\cos(\Theta) + 0.08\cos(3\Theta)\cos(\Theta)\,; \\ & y = 0.05 + 0.65\sin(\Theta) - 0.25\cos(\Theta)\sin(\Theta) \\ & - 0.15\sin^2(\Theta) + 0.08\cos(3\Theta)\sin(\Theta)\big),\ \Theta \in [0, 2\pi[\Big\},\end{aligned}$$

pictured in black below.

The incident field u_{i} is assumed to come from $\theta_{\mathrm{i}} = 45°$ (inside the convexity of the target), with a frequency of 3 MHz. The maximal number of iterations for the optimization loop is fixed to 200. One could also adjust a stopping criterion on the accuracy of the results. Here the center is searched for 5 iterations, then the radius is modified, and a Fourier mode is added each $N_p = 15$ iterations.

B. With a noisy measurement g

In these first tests, we consider the case of a perfectly known h but a noisy measurement g. More precisely, we consider g of the following form :

$$g(\omega) = g_{\mathrm{dir}} + \sum_{i=1}^{4} \beta_g \sin(i\phi) Y_i(\omega), \tag{9}$$

where g_{dir} corresponds from artificial measurements computed through the direct problem (1), ϕ to the angle at the position (x_X, y_X), and β_g to a noise scaling function with respect to the real data g_{dir}. This latter obviously meets the assumptions introduced in Section III.

The results are pictured in Fig. 2. First, in (a) we plot the obtained shapes computed with the robust (in dotted lines) and usual (in dashed lines) methods, when 0%, 5% and 10% of noise levels are considered. Second, in (b) the corresponding value of the cost functionals $\mathfrak{K}$ (in dotted lines) and $\mathcal{K}$ (in dashed lines) with respect to the iterations are pictured.

In this case, the robust method demonstrates its effectiveness. As depicted in Fig. 2 (a), even with a 5% noise level, the results outperform those obtained using the functional $\mathcal{K}$. The reconstruction is nearly as precise as in noise-free conditions. Moreover, with a 10% noise level, the robust method produces results comparable to those achieved with the classical method under 5% noise conditions. These observations are supported by the behavior of the functionals $\mathfrak{K}$ and $\mathcal{K}$. Notably, as the noise level increases, $\mathcal{K}$ exhibits a rapid escalation, whereas $\mathfrak{K}$ displays a relatively muted response.

C. With noisy data g and h

In this second test, we consider that both the measurement and the incident wave, that is g and h, are noisy. More precisely, we consider the same noisy measurement g as

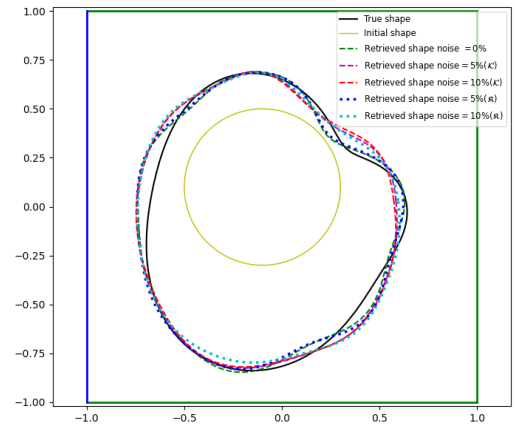

(a) Real and retrieved objects for different levels of noise

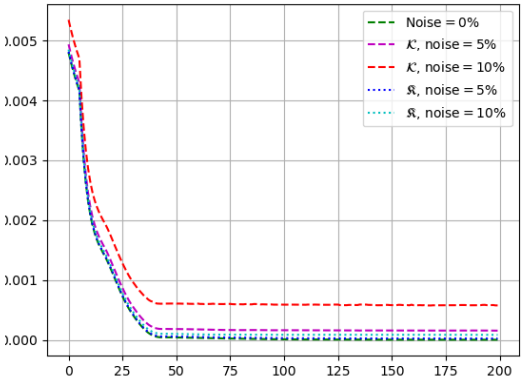

(b) The corresponding value of the cost functional $\mathfrak{K}$

Fig. 2: Reconstruction of the PEC with a noisy measurement g.

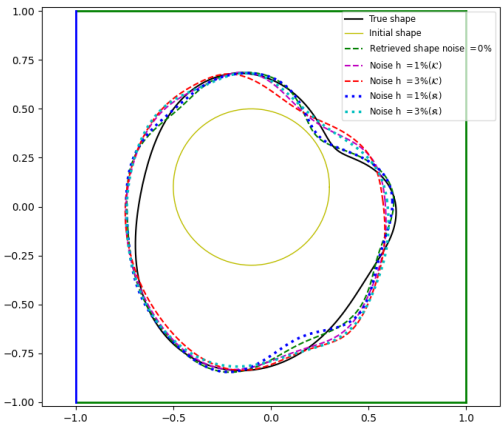

(a) Real and retrieved objects for different levels of noise

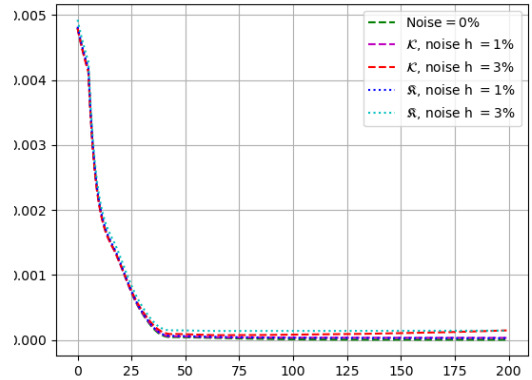

(b) The corresponding value of the cost functional $\mathfrak{K}$

Fig. 3: Reconstruction of the PEC with noisy data g and h.

above (see (9)) with a fixed noise level of 5%. We add here the assumption that the amplitude contains noise and thus h is of the following form

$$h(\omega) = j(k - \mathbf{k}_{\mathrm{i}}(\theta_{\mathrm{i}}) \cdot \mathbf{n}) u_{\mathrm{i}_0} \exp(-j\mathbf{k}_{\mathrm{i}}(\theta_{\mathrm{i}}) \cdot \mathbf{r}) + j(k - \mathbf{k}_{\mathrm{i}}(\theta_{\mathrm{i}}) \cdot \mathbf{n}) \beta_h \sum_{k=1}^{4} \sin(k\phi) Y_k(\omega) \exp(-j\mathbf{k}_{\mathrm{i}}(\theta_{\mathrm{i}}) \cdot \mathbf{r}),$$

where u_{i_0} is the true amplitude, and β_h a noise scaling coefficient with respect to the norm of h. Thus, the assumptions of Section III are met. Note that taking into account noise on h has more influence than on g since the boundary condition h intervenes in the resolution of all the problems solved by u_{D_i} and u_{R_i} (while g only appears in the problems solved by u_{D_i}).

The results are pictured in Fig. 3. As previously, we plot in (a) the obtained shapes with both the robust (in dotted lines) and the conventional method (in dashed lines) for different noise levels on h, i.e., 1% and 3%. In (b), the values of the cost functions $\mathfrak{K}$ (in dotted lines) and $\mathcal{K}$ (in dashed lines) with respect to the number of iterations and for the different levels of noise are pictured.

As expected, it can be observed that the reconstruction of the shape seems to be more sensitive with respect to the noise on h. Nevertheless, the reconstruction is still suitable, at least for 3% of noise on h, and the robust method allows a better reconstruction. We can notice that in practice, the incident wave is quite well known and thus the level of noise on h is quite small (less than 3%). One can also note from Fig. 3 (b) that the functional without using the robust method starts to increase at 3% of noise on h.

V. Conclusion

In this article, we derived a robust method to retrieve the shape of a metallic target from noisy electromagnetic measurements. A parametric shape optimization procedure was used and the expectation of the Kohn-Vogelius functional was minimized. Using the Karhunen-Loève expansion, we obtained a deterministic expression for the cost function from which we computed the shape gradient and obtained a descent direction. Then, we employed a Nesterov gradient scheme to tackle the resulting deterministic problem.

Numerical experiments have been performed under different scenarios. Firstly, we considered the case where only the measurements had noise. The robust method showed

promising results, outperforming the non-robust approach in terms of reconstruction accuracy. Secondly, we assumed that both the measurements and the incident wave contained noise. In this case, the results are still better with the robust method, but the latter seems to be more sensitive to a completely noisy setup.

In future work, we plan to investigate another objective robust functional that combines the first and second-order moments of the random Kohn-Vogelius cost functional. In addition, the case of multiple sources and multiple receivers is also being studied to have a more accurate model. Finally, we will consider the case where the target is not a PEC in a forthcoming work.

REFERENCES

[1] M. Prickett and C. Chen, "Principles of inverse synthetic aperture radar/isar/imaging," in *EASCON'80; Electronics and Aerospace Systems Conference*, pp. 340–345, 1980.

[2] A. Litman, D. Lesselier, and F. Santosa, "Reconstruction of a two-dimensional binary obstacle by controlled evolution of a level-set," *Inverse Problems*, vol. 14, pp. 685–706, June 1998.

[3] F. Comblet, A. Khenchaf, A. Baussard, and F. Pellen, "Bistatic synthetic aperture radar imaging: Theory, simulations, and validations," *IEEE Transactions on Antennas and Propagation*, vol. 54, no. 11, pp. 3529–3540, 2006.

[4] O. Dorn and D. Lesselier, "Level set methods for inverse scattering," *Inverse Problems*, vol. 22, pp. R67–R131, Aug. 2006.

[5] G. R. Feijóo, A. A. Oberai, and P. M. Pinsky, "An application of shape optimization in the solution of inverse acoustic scattering problems," *Inverse Problems*, vol. 20, pp. 199–228, Dec. 2003. Publisher: IOP Publishing.

[6] G. R. Feijoo, "A new method in inverse scattering based on the topological derivative," *Inverse Problems*, vol. 20, pp. 1819–1840, Dec. 2004.

[7] L. Audibert, H. Haddar, and X. Liu, "An accelerated level-set method for inverse scattering problems," *SIAM Journal on Imaging Sciences*, vol. 15, no. 3, pp. 1576–1600, 2022.

[8] M. Benedetti, D. Lesselier, M. Lambert, and A. Massa, "A multi-resolution technique based on shape optimization for the reconstruction of homogeneous dielectric objects," *Inverse Problems*, vol. 25, p. 015009, Jan. 2009.

[9] M. Dambrine and V. Karnaev, "Robust obstacle reconstruction in an elastic medium," *Discrete and Continuous Dynamical Systems - B*, 2023.

[10] F. Caubet, M. Dambrine, D. Kateb, and C. Z. Timimoun, "A Kohn-Vogelius formulation to detect an obstacle immersed in a fluid," *Inverse Problems & Imaging*, vol. 7, no. 1, p. 123, 2013.

[11] T. Bonnafont and F. Caubet, "Inverse scattering using a kohn-vogelius formulation and shape optimization method," in *2023 17th European Conference on Antennas and Propagation (EuCAP)*, pp. 1–5, IEEE, 2023.

[12] A. Henrot and M. Pierre, *Variation et optimisation de formes: une analyse géométrique*. No. 48 in Mathématiques & applications, Berlin Heidelberg New York: Springer, 2005.

[13] G. Allaire and M. Schoenauer, *Conception optimale de structures*, vol. 58. Springer, 2007.

[14] F. Hecht, O. Pironneau, A. Le Hyaric, and K. Ohtsuka, "Freefem++ manual," 2005.